ANNALS OF GEOPHYSICS, 67, 4, DM434, 2024; doi:10.4401/ag-9138
OPEN ACCESS

Developing Liquefaction Prediction Equations for Gravels Based on DPT Blow Count and Shear Wave Velocity at Field Case History Sites

Kyle Rollins[*,1] and Jashod Roy[2]

(1) Brigham Young University, Civil & Construction Engineering, Provo, USA
(2) Kiewit Engineering, Omaha, USA

Article history: received August 112, 2024; accepted September 9, 2024

Abstract

Gravelly soils have liquefied at multiple sites in at least 20 earthquakes over the past 130 years. These gravels typically contain more than 25% sand which lowers the permeability and makes them susceptible to liquefaction. In other cases, a low permeability layer at the surface impedes drainage and causes liquefaction. Typical SPT- or CPT-based liquefaction correlations can be affected by large gravel particles and lead to erroneous results. To deal with these problems, we have developed liquefaction triggering curves for gravelly soils based on (1) shear wave velocity (V_s) and (2) a 74-mm diameter dynamic cone penetrometer (DPT), that are less affected by gravel particles. These correlations are based on case histories where gravel did and did not liquefy in past earthquakes. The V_S-based liquefaction triggering curves for gravels shift to the right relative to similar curves based on sands. Good agreement has been obtained with liquefaction resistance from the DPT and the CPT when these methods could all penetrate the gravel in Wellington New Zealand. Correlations are developed between V_s and blow count from the DPT.

Keywords: Dynamic Cone Penetrometer; Gravel; Liquefaction; Shear wave velocity

1. Introduction

Liquefaction of loose saturated granular soils results in significant damage to civil infrastructure such as buildings, bridges, roadways, pipelines, and ports in nearly every earthquake. Liquefaction and the resulting loss of shear strength can lead to landslides, lateral spreading, loss of vertical and lateral bearing support for foundations, and excessive foundation settlement and rotation. Direct and indirect economic losses resulting from liquefaction are substantial costs to society. Although liquefaction has primarily been associated with sands and silty sands, a growing body of evidence indicates that gravelly soils can also be susceptible to liquefaction. A significant number of gravel liquefaction case histories have occurred during more than 20 earthquake events over the past 130 years. Engineers have sometimes been sceptical about gravel liquefaction because gravels typically have high hydraulic conductivities or Darcy permeability coefficients (k). For example, Seed et al. (1976), using numerical modeling, found that gravels with a hydraulic conductivity higher than 0.004 m/sec would likely dissipate excess pore pressures

as rapidly as they were degenerated by typical earthquake shaking. Nevertheless, over the past 15 years, gravel liquefaction has caused significant damage to ports in Cephalonia, Greece (Athanasopoulos-Zekkos et al., 2019); Iquique, Chile (Rollins et al., 2014); Manta, Ecuador (Sebastian-Lopez et al., 2018), and Wellington, New Zealand (Cubrinovski et al., 2017). Likewise, older dams that were constructed on gravelly soil foundations or with poorly compacted gravel are now being evaluated to consider the potential for liquefaction. Gravel liquefaction assessment for older dams and ports along with the selection of appropriate remedial measures are often multi-million-dollar decisions. These decisions involve both life-safety and regional economic issues. Moreover, gravel liquefaction must be routinely evaluated for a wide range of small to medium-size projects around the world.

2. Liquefaction Susceptibility for Gravelly Soils

A review of case histories where gravelly soils have liquefied makes it possible to examine the variation of grain-size distributions curves for these soils. Grain-size distribution curves for several case histories where gravelly soils have liquefied in past earthquakes are plotted in Fig. 1 (Rollins et al., 2021). It can be observed that there is considerable variation in these curves. However, the curves typically involve well-graded materials. Even though the curves may indicate more than 50% gravel size particles (> 4.75 mm) so that the soil classifies as gravel (according to the Unified Soil Classification system, for example), there is typically more than 30% sand content and fines content ranges from 0 to 22%. The sand contents and fines contents for these soils would be expected to reduce the hydraulic conductivity of these soils considerably, relative to a clean gravel, as the D_{10} size decreases.

Research on the hydraulic conductivity of sand-gravel mixtures reported by She et al. (2006), indicates that the hydraulic conductivity decreases significantly as sand content increases to about 25 to 30%. With this percentage, the void spaces in the gravel particles become filled with sand and control the hydraulic conductivity of the overall mixture. As a result, the hydraulic conductivity can decrease by 1.5 to 3.5 orders of magnitude as the as shown in Fig. 2, depending on the grain size of the sand involved. Although the hydraulic conductivity of the clean gravel may be above the 0.004 m/sec boundary precluding liquefaction, as defined by Seed et al. (1976), the hydraulic conductivity of the sand-gravel mixture could be more typical of sand than of gravel. Therefore, excess pore pressures could develop in a sandy gravel layer without a low permeability layer impeding drainage of the layer.

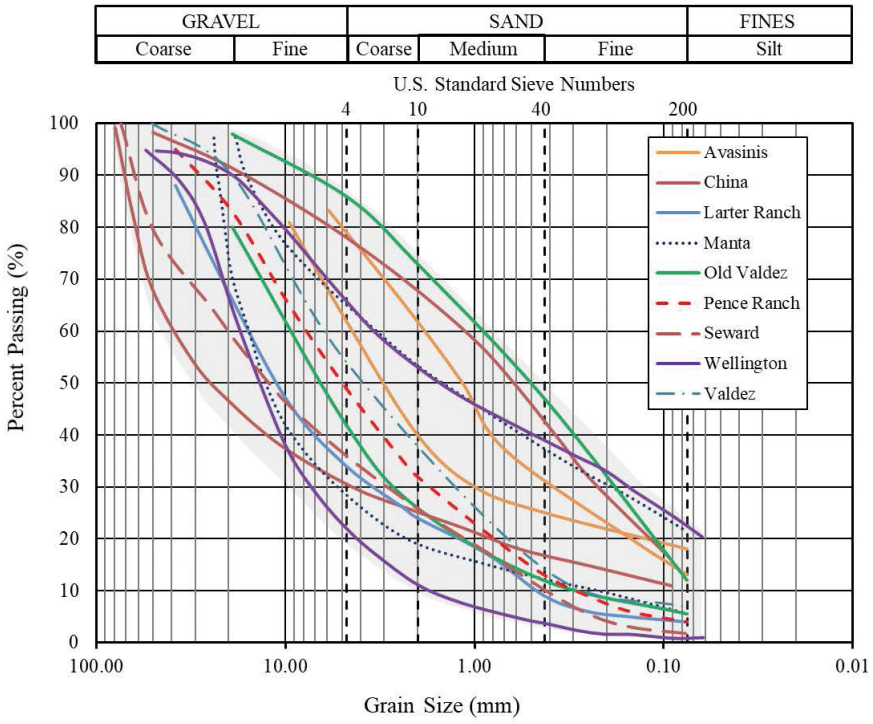

Figure 1. Particle-size distribution curves for sites where gravelly soils have been observed to liquefy during earthquake shaking.

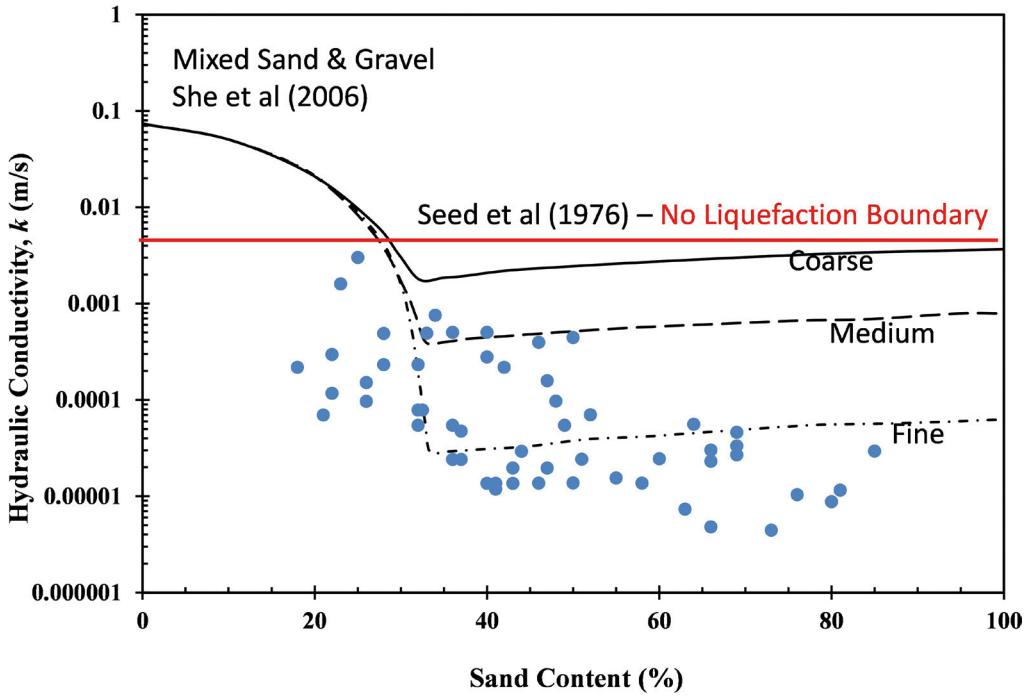

Figure 2. Hydraulic conductivity variation of sand-gravel mixtures versus sand content reported by She et al. (2006) along with hydraulic conductivity versus sand content for gravel liquefaction case histories (blue dots) from the literature.

While measurements of the hydraulic conductivities at all the gravel liquefaction sites are not presently available, it is possible to make estimates of the hydraulic conductivity using the Kozeny-Karmen equation given by,

$$k = \frac{g}{v}(8.3 \times 10^{-3})\left[\frac{n^3}{(1-n)^2}\right]D_{10}^2 \quad (1)$$

where g is the acceleration of gravity, v is the dynamic viscosity, n is the porosity, and D_{10} is the particles for which 10 percent is finer. Using this approach, the estimated hydraulic conductivity for gravel liquefaction case histories are plotted versus sand content in Fig. 2. A review of the data points indicates that all the points fall below the k = 0.004 m/sec boundary precluding liquefaction, although a few points from China fall just below the boundary. Of course, data points with a *k* value below the boundary may still not liquefy if the earthquake shaking is not strong enough relative to the density of the gravel.

In several gravel liquefaction case histories there is evidence of a low hydraulic conductivity layer overlying the liquefied gravel layer that may have impeded pore pressure dissipation and increased the potential for liquefaction. These lower permeability layers have included: (1) natural deposits of silt and clay with low hydraulic conductivity such as in the Chengdu Plain of China (Cao et al., 2013) and Armenia (Yegian et al., 1994), (2) concrete pavements at ports such as Centreport in Wellington, New Zealand (Cubrinovski et al. 2017), and (3) concrete floors slabs for building such as in Avasinis, Italy (Rollins et al., 2021; Sirovich, 1996). Numerical analyses reported by Roy et al. (2022) indicate that a low permeability layer can be relatively thin and does not necessarily need to be impervious to impede drainage sufficiently to produced liquefaction in the underlying gravel layer. Impeded drainage can lead to liquefaction in the underlying gravel even if the k value is higher than 0.004 m/sec, although the thickness of the liquefied zone may be limited to a relatively thin layer immediately below the low permeability layer depending on the permeability and duration of the earthquake shaking.

In summary, as illustrated in Fig. 3, gravel liquefaction can occur in two types of soil profiles. In case (a), the sandy gravel layer contains sufficient sand and/or fines to reduce the hydraulic conductivity of the gravel to that of sand and can liquefy. In case (b) a low k value layer impedes drainage of the underlying gravel layer such that excess pore pressure can develop in the underlying layer and liquefy.

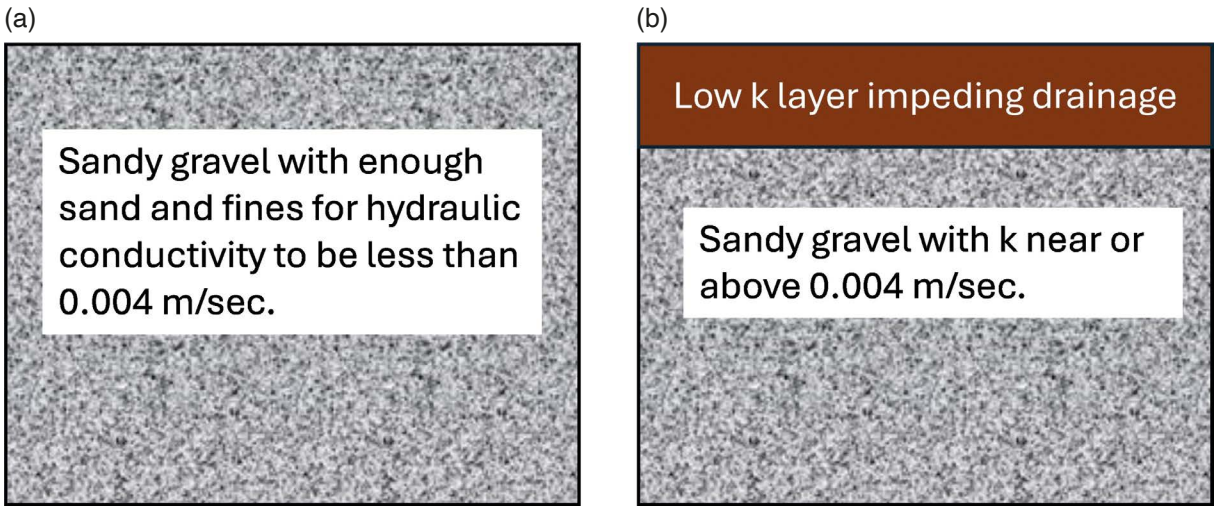

Figure 3. Gravel layers that are susceptible to liquefaction: (a) sandy gravel with lower hydraulic conductivity and (b) gravel with higher hydraulic conductivity but with a low hydraulic conductivity layer that impedes drainage.

3. Penetration Testing Methods for Evaluating Gravel Liquefaction

The large particle size of gravels can lead to artificially high penetration resistance values from traditional in situ tests such as the cone penetrometer (CPT) test and the Standard Penetration (SPT) test (DeJong et al., 2017). The 168 mm diameter Becker Penetration Test (BPT) (Harder and Seed, 1986; Harder, 1997) reduces the potential for artificially high penetration values; however, this method is relatively expensive and is not available outside of North America. In addition, the method uses a correlation between the BPT blow count and the SPT blow count which introduces another layer of uncertainty relative to methods that directly correlate blow count with the cyclic resistance to liquefaction.

Chinese engineers in the Chengdu region, dealing with extensive gravel deposits, developed a dynamic done penetrometer test (DPT) using a 74 mm diameter cone tip which tapers to a 60 mm drill rod to reduce rod friction as shown in Fig. 4 (Chinese design code, 2001). The DPT blow count, N_{120}, represents the number of hammer blows to drive the penetrometer 30 cm with a 120 kg hammer dropped from a height of 1 m. Raw blow counts are typically reported at every 10 cm of penetration, but are multiplied by three to get the equivalent N_{120} for 30 cm of penetration. This test is a large-size implementation of the lightweight dynamic cone penetrometer that is used extensively for assessment of compaction of soils in pavement applications (ASTM, 2018). A variety of different cone geometries are also known as dynamic probing in Europe (British Standards 2012). In the Chinese version of the DPT, the cone tip is driven continuously with a 120 kg hammer dropped from one meter and is capable of penetrating medium to dense gravel and cobbles. DPT soundings can be easily performed with conventional SPT drilling rigs or even simple tripod systems, making it viable worldwide.

The DPT does not produce a sample or identify the soil like the CPT, therefore, a companion borehole is necessary to classify the soil accurately and provide grain-size distribution curves. Refusal is typically designated at 40 blows per 10 cm. However, if the companion soil boring indicates that looser liquefiable gravel is expected at a greater depth, the hole can be advanced through the dense zone using conventional drilling and the DPT test can then be resumed.

At 74 mm, the DPT diameter is 50% larger than the SPT and 110% larger than a standard 10 cm^2 CPT; however, it is still 55% smaller than the BPT. Although the BPT provides the largest diameter to particle size ratio of all tests, the DPT is superior to the SPT or CPT and could be a reasonable solution in many cases depending on the gravel size and percentage. Based on discrete element modeling, Iqbal (2004) indicates that a CPT q_c begins to be influenced by particle size when the D_{50} of the soil exceeds 30% of the cone diameter. If this criterion is applicable to the DPT, then the blow count would start to be affected when the D_{50} exceeds 22 mm. The D_{50} for nearly all of the grain size curves from gravel liquefaction case histories in Fig. 1 are smaller than this value.

Chinese experience suggests that rod friction can become a problem when penetration depths exceed 20 m or when penetrating soft silts and clays at shallower depths. In these cases, it may be necessary to use casing to

eliminate rod friction and drive the cone through the bottom of the casing. Rod friction became a problem at gravel liquefaction sites in Croatia within a saturated clayey silt to clay layer near the surface that was 5 to 9 meters thick (Rollins et al., 2024). In these cases, it was necessary to case through the clay layer or to use a device to measure the reduction in energy resulting from rod friction so that this effect could be corrected.

Based on field case histories of gravel liquefaction in the M_w 7.9 Wenchuan earthquake, Cao et al. (2013) developed probabilistic liquefaction triggering curves for gravels based on the DPT blow count. However, these curves are based on relatively few data points from one earthquake and a geologic profile consisting of loose alluvial fan gravel layers overlain by a clay surface layer typically 2- to 4-m thick (Cao et al., 2013). Because of the limited number of data points and the possibility of false negatives (sites where liquefaction may have occurred but did not produce surface manifestation), the triggering curves for 85 and 15% probability of liquefaction were widely separated. In contrast, more mature probabilistic liquefaction triggering curves for sands based on the CPT (Boulanger and Idriss, 2014) have more closely grouped probability curves because the data set is larger. Therefore, it becomes crucial to add more case histories to the DPT database from different geologic settings. In addition, the Cao et al. (2013) triggering curves were developed for a single event of M_w 7.9 without incorporating any correction to the seismic demand by using the Magnitude Scaling Factor (*MSF*). Thus, applicability of these curves would become questionable for evaluating the liquefaction potential of gravelly soils with different magnitudes. Therefore, additional data points from earthquakes with different magnitudes are useful in developing an improved DPT-based liquefaction triggering procedure and a gravel-based MSF curve.

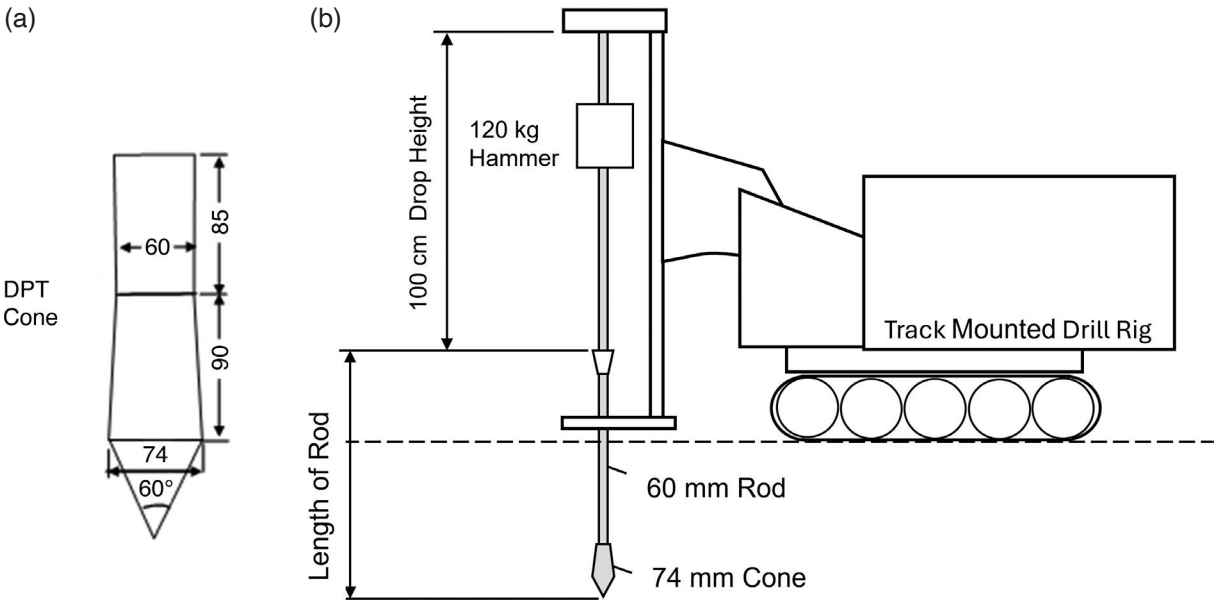

Figure 4. Schematic drawing of (a) DPT cone penetrometer (dimensions in mm) and (b) drill rig with hammer and drop height for DPT.

4. Shear Wave Velocity Test Methods for Evaluating Gravel Liquefaction

As an alternative to penetration resistance testing, in situ measurement of shear wave velocity (V_s) is a popular way of characterizing the liquefaction resistance of soil deposits. V_s is a basic mechanical property of soils, directly related to the small strain shear modulus (G_0), that is an essential parameter for performing soil-structure interaction analysis that can also be used to estimate liquefaction resistance. The use of V_s as a field index of liquefaction resistance is based on the recognition that both V_s and liquefaction resistance are similarly, but not proportionally, influenced by void ratio, effective confining stresses, stress history and geologic age (Youd et al., 2001). In addition, V_s is considerably less sensitive to the problems of soil compression and reduced penetration resistance when fines are present, compared with SPT and CPT methods. Therefore, V_s requires only minor corrections for fines content (*FC*) at least for sands (Kayen et al., 2013). The primary advantage of the in-situ V_s approach is that testing

can be performed at sites where borings are not possible, or the penetration test results may be unreliable. Hence, V_s measurement can be considered as a reliable and economical alternative to overcome the difficulties of penetration testing within gravelly strata.

The traditional methods of measuring V_s require a penetrometer or instrumented boreholes to measure the travel time of shear waves at various depths. A downhole test requires one borehole to measure the vertically propagating wave, while a cross-hole test requires at least two boreholes to directly measure the horizontally propagating wave (Stokoe et al., 1994). These invasive test methods are usually quite expensive due to the cost of drilling, casing, and grouting boreholes, but they provide direct velocity measurements at depth intervals of 1 to 1.5 m. In the last two decades, advanced non-invasive test methods, Spectral Analysis of Surface Waves (SASW) and Multichannel Analysis of Surface Wave (MASW) have been developed, which indirectly estimate the V_s through the surface wave dispersion characteristics of the ground (Andrus, 1994; Kayen et al., 2013; Stokoe et al., 2004). These non-invasive test methods have significantly reduced the cost of in-situ V_s estimation and made soil exploration possible at sites where penetration is not possible or economically feasible. Unfortunately, the velocity profiles provided by these indirect measurements involve significant uncertainly because the solutions are not unique. For example, different velocity profiles can be developed depending on the number and thickness of the layers used in developing the profile (Vantassel and Cox, 2022). When using velocity profiles from MASW for liquefaction assessments, it may be difficult to isolate thinner liquefiable layers because of averaging within an assumed layer without additional geotechnical information. Significant improvements in velocity profile estimation can be achieved if a companion borehole is available to define the soil profile and relative stiffness values. Therefore, this practice is recommended for liquefaction evaluations.

Andrus and Stokoe (2000) collected a large database of V_s profiles from locations around the world where both sandy and gravelly soils had liquefied in various earthquakes. Based on this dataset, improved triggering curves were developed for sands and gravels for different fines contents. The database of Andrus and Stokoe (2000) only contained a limited number of data points where the V_{s1} (V_s normalized for vertical stress of 100 kPa as discussed subsequently) was higher than 200 m/s even for gravelly soils. This is consistent with observations by Kokusho et al. (1995) that loose gravels, even though well-graded, can exhibit shear wave velocities similar to those of loose sands. In contrast, the SPT-V_s correlation by Ohta and Goto (1978) and the correlation by Rollins et al. (1998b) suggest a higher range of V_{s1} (230 m/s) for liquefiable Holocene gravels. Such variation of shear wave velocity in gravelly soils can be due to variations in gravel content, grain size distribution, and the relative density of the soil matrix (Kokusho et al., 1997; Weston, 1996; Chang, 2016; Chen et al., 2018.)

Cao et al. (2011) developed probabilistic liquefaction triggering curves for gravels using logistic regression techniques based on V_S data collected from the Chengdu plain in China where gravel liquefaction took place during the 2008 Wenchuan earthquake. These curves are based on 47 data points (19 liquefaction and 28 no liquefaction points) that refer to a single earthquake and a similar geological environment (Cao et al., 2011). Because of the limited number of data points and the possibility of false negatives (sites where liquefaction may have occurred but did not produce surface manifestation), the range between the 15% to 85% probability of liquefaction are relatively far apart. In contrast, Vs-based probabilistic liquefaction triggering curves for sands (Kayen et al., 2013) have more closely grouped probability curves because of the larger data set. Moreover, the Cao et al. (2011) triggering curves were developed for a single event of M_W 7.9 without proposing any correction to the seismic demand for different earthquake magnitudes. Thus, the applicability of these curves becomes questionable for evaluating the liquefaction potential of gravelly soils for other seismic events of different magnitude. Although existing *MSF* models developed for sand liquefaction (Youd et al., 2001) can be used, it is unclear whether they are appropriate for gravel liquefaction assessment based on *Vs*. Therefore, additional effort is necessary to collect more *Vs* data from the gravel liquefaction sites to improve the existing *Vs*-based liquefaction triggering curves for gravelly soils.

5. Collection of Additional Gravel Case History Data

In the present study, a larger database consisting of 174 V_s data points and 137 DPT data points has been compiled by collecting additional data points from seven different countries around the world where gravel liquefaction did or did not take place in 17 major earthquake events and adding them to the existing data points from China reported by Cao et al. (2011; 2013). Case histories with no liquefaction in Italy, Greece, and New Zealand were strategically identified, tested, and then added to the database to help constrain the position of the liquefaction triggering curves.

For each case history, the cyclic stress ratio (CSR) has been obtained by using the simplified equation

$$CSR = 0.65(a_{max}/g)(\sigma_{vo}/\sigma'_{vo})r_d \tag{2}$$

originally developed by Seed and Idriss (1971) where a_{max} is the peak ground acceleration, σ_{vo} is the initial vertical total stress, σ'_{vo} is the initial vertical effective stress, and r_d is a variable that accounts for the flexibility of the soil versus depth which was updated to include the effect of both depth and earthquake magnitude using the equation

$$r_d = e^{[\alpha(z)+\beta(z)M_w]} \tag{3}$$

where:

$$\alpha(z) = -1.012 - 1.126sin\left({}^{z}/_{11.73} + 5.133\right) \tag{4}$$

$$\beta(z) = 0.106 + 0.118sin\left({}^{z}/_{11.28} + 5.142\right) \tag{5}$$

and z is the depth in meters, based on the work by Golezorkhi (1989) and Idriss (1999).

Peak ground accelerations (*PGA* or a_{max}) for every location were taken from the literature or from USGS Shake Maps (Worden et al., 2010) where necessary as was done by Idriss and Boulanger (2008) for their CPT database. Besides *CSR*, the moment magnitude (M_w) has been considered as another independent seismic variable for obtaining the liquefaction potential of gravelly soils. Values of M_w were found from available references regarding the appropriate earthquake. The data set contains a wide distribution of M_w ranging from 5.3 to 9.2 as well as *PGA* ranging from 0.17 to 0.6 g.

5.1 Corrections for DPT Blow count

The DPT blow count, N_{120}, represents the number of hammer blows to drive the penetrometer 30 cm with a 120 kg hammer dropped from a height of 1 m. Based on 1200 hammer energy measurements, Cao et al. (2012) found that the Chinese DPT provided an average of 89% of the theoretical free-fall energy. Since the energy delivered by a given hammer (E_{Hammer}) was different than the energy actually supplied by a Chinese DPT hammer ($E_{Chinese\ DPT}$), it is often necessary to correct the measured blow count. To obtain E_{Hammer} it is typically necessary to measure the energy transferred to the drill rod using a SPT hammer analyzer, which is less than the theoretical energy due to friction losses. In this study, the correction was made using the simple linear reduction s ggested by Seed et al. (1985) for SPT testing,

$$N_{120} = N_{Hammer} \cdot (E_{Hammer}/E_{Chinese\ DPT}) \tag{6}$$

where N_{Hammer} is the number of blows per 0.3 m of penetration obtained with a hammer delivering an energy of E_{Hammer} . In addition, Cao et al. (2013) recommend an overburden correction factor, C_n, to obtain the normalized N'_{120} value using the equation

$$N'_{120} = N_{120} \cdot C_n \tag{7}$$

where

$$C_n = (100/\sigma'_{vo})^{0.5} \leq 1.7 \tag{8}$$

and σ'_{vo} is the initial vertical effective stress in kN/m^2. In the current study, a limiting value of 1.7 was added to be

consistent with the C_n used to correct penetration resistance from other in-situ tests (Youd et al., 2001). For each case history, a critical layer was selected below the water table and with the lowest ratio of blow count divided by CSR over at least one meter. All the critical liquefaction layers were located at depths less than about 14 m which is consistent with other liquefaction case history databases and with blow counts typically less than about 20.

5.2 Corrections for Shear Wave Velocity

The V_S values obtained by various in-situ methods were corrected for overburden pressure to obtain V_{s1} using the equation:

$$V_{s1} = V_s \cdot (P_a/\sigma'_{vo})^{0.25} \tag{9}$$

where σ'_{vo} is the initial vertical effective stress, and P_a is atmospheric pressure approximated by a value of 100 kPa as suggested by Sykora (1987) and adopted by Youd et al. (2001). These normalized V_{s1} profiles based on the V_s testing were then plotted as a function of depth and a critical depth with the lowest average ratio of V_{s1}/CSR over a length of at least one meter. Once again, the critical layers based on V_{s1} were all shallower than 14 m.

6. Development of Probabilistic Liquefaction Triggering Curves

Based on the new expanded database, a new set of probabilistic liquefaction triggering curves has been developed by logistic regression analysis based on V_{s1} and also N'_{120}. The triggering equations developed in the present study include the earthquake magnitude as an independent variable.

6.1 Probabilistic DPT-Based Liquefaction Triggering Curves

The logistical regression analysis was carried out using M_w, N'_{120}, and ln(CSR) as independent variables and the following equation was developed to calculated the Cyclic Resistance Ratio (CRR)

$$CRR = exp\left[\frac{1.32M_w - 0.0008N'^3_{120} - \ln\left(\frac{1-P_L}{P_L}\right)}{5.2}\right] \tag{10}$$

where P_L is the probability of liquefaction expressed as a fraction. If a given probability and M_w of 7.5 is used in Eq. (9), a plot of $CRR_{M=7.5}$ vs. N'_{120} can be produced for a given probability. Figure 5 provides a plot of $CRR_{M=7.5}$. N'_{120} for a M_w 7.5 for various P_L values. The $CSR_{M=7.5}$ and N'_{120} data points for each liquefaction and no liquefaction case history are also shown in Fig. 5 relative to the triggering curves proposed by Rollins et al. (2021). The procedure for converting the CSR for a given earthquake to that for a $M_w = 7.5$ using the MSF is discussed subsequently.

Roy et al. (2023) report that the CRRs obtained from the CPT and the DPT in gravelly fill at the Centre Port in Wellington, were in good agreement throughout the depth where the CPT could penetrate. Occasional spikes in the CPT q_c due to interference with large gravel particles were not observed in the DPT N'_{120} profiles. In addition, the factors of safety correctly indicated liquefaction or no liquefaction in three earthquakes that struck the port. This agreement between methods developed with different data sets and interpretation methods provides confidence in the reliability of the DPT triggering curves.

6.2 Probabilistic V_S-Based Liquefaction Triggering Curves

Logistical regression analysis was also carried out using M_w, V_{s1} and ln(CSR) as independent variables and the following equation was developed to calculated the Cyclic Resistance Ratio (CRR)

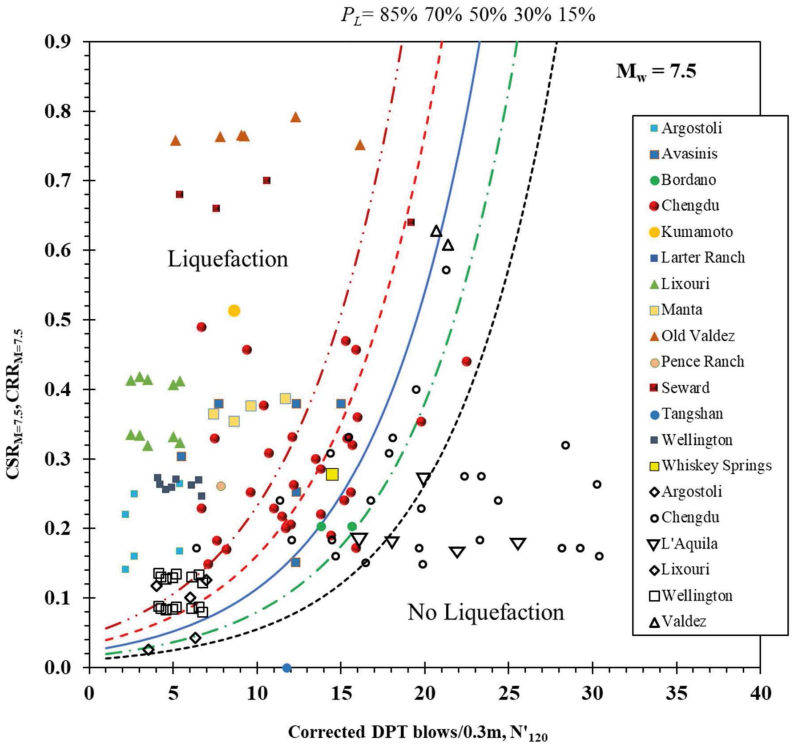

Figure 5. Plot of *CRR* vs. N'_{120} for a M_w 7.5 earthquake with various probabilities of liquefaction based on expanded DPT-based database proposed by Rollins et al. (2021) along with $CSR_{Mw=7.5}$ and N'_{120} points from case histories.

$$CRR = exp\left[\frac{1.438M_w - 3.8x10^{-7}V_{s1}^3 - \ln\left(\frac{1-P_L}{P_L}\right)}{4.026}\right] \quad (11)$$

where P_L is the probability of liquefaction expressed as a fraction. If a given probability and M_w of 7.5 is used in Eq. (10), a plot of *CRR* vs. V_{s1} can be produced for a given probability. Figure 6 provides a plot of *CRR* vs. V_{s1} for M_w 7.5 for various P_L values proposed by Rollins et al. (2022).

The new probabilistic triggering curves with liquefaction probabilities of 15% to 85% are plotted in Fig. 7a with solid lines along with similar curves developed by Cao et al. (2011) with dashed lines to draw a distinct comparison between the two triggering procedures. For lower values of V_{s1} (around 150 m/s), the *CRR* for the new 50% probability of liquefaction curve is about 0.10 while it is only 0.04 for the Cao et al. (2011) curves. This adjustment produces much better agreement with observed field performance.

This higher *CRR* value at small velocities is also more typical of that predicted by the V_s-based triggering curves developed by Kayen et al. (2013). The data points from the Port of Wellington where liquefaction did not take place during the Cook Strait and Lake Grassmere earthquakes (both $M_w = 6.6$) in 2013 and the "no liquefaction" points from Argostoli, KNK and Coyote Creek have had a significant effect in constraining the lower branch of the triggering curves to move upwards. Likewise, the triggering curves at the higher range of V_{s1} values have been tightened relative to the curves developed by Cao et al. (2011) as a result of the additional "no liquefaction" data points from Chengdu, L'Aquila and Valdez. Additional data points would certainly be desirable to define the shape of the curve better in this range of V_{s1} values.

In the middle range of the curve, a few "no liquefaction" points from the Chengdu plain fall above the 70% triggering curve and some liquefaction points from the same region fall below the 30% triggering curve. These points may belong to the false negative or false positive categories leading to inconsistent evaluation of the actual incident. Due to the presence of these points, the set of triggering curves develop a slightly sloped shape above a V_{s1} value of 200 m/s such that some "no liquefaction" points fall marginally on the 30% triggering curve instead of falling distinctly below this line.

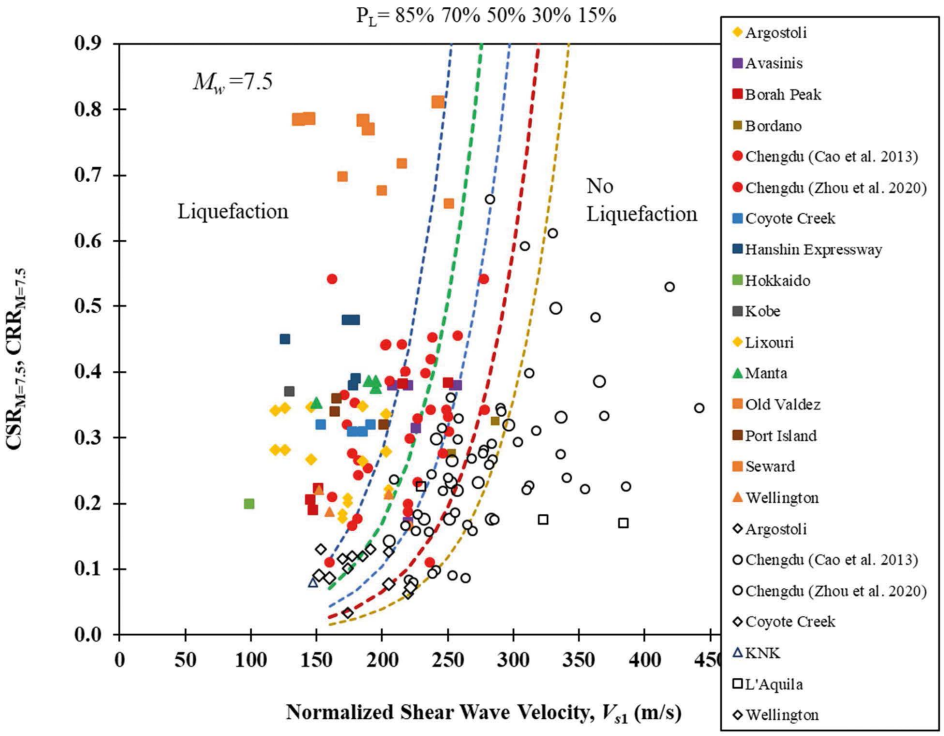

Figure 6. Plot of CRR vs. V_{s1} for a M_w 7.5 earthquake with various probabilities of liquefaction based on expanded V_S-based database collected by Rollins et al. (2022) along with $CSR_{Mw=7.5}$ and V_{s1} points from case histories.

As shown in Fig. 7a, for V_{s1} values above 200 m/s, the $P_L = 50\%$ curve for the new regression is very similar to that for the Cao et al. (2011) regression. However, the addition of new liquefaction points has pulled the new $P_L = 85\%$ curve to the right while the addition of no-liquefaction data points has pulled the new $P_L = 15\%$ curve to the left, relative to the Cao et al. (2011) curves.

Moving the new $P_L = 15\%$ curve to the left is particularly significant because this curve is often recommended for deterministic evaluations (Kayen et al., 2013). However, the slope of the new set of curves from this study remains almost the same as for the Cao et al. (2011) curves. Overall, the spread between the triggering curves for various probabilities of liquefaction is substantially reduced for the new triggering curves relative to the Cao et al. (2011) curves. This result is consistent with the concept that the increased number of data points reduces the uncertainty that develops when an individual data point plots in an unexpected position. Furthermore, the addition of data points where liquefaction did not occur has helped constrain the triggering curves on the "no liquefaction side" in critical locations.

A comparison is provided between the newly developed triggering curves for gravel and the curves developed by Kayen et al. (2013) for sand in Fig. 7b. To plot the triggering curves for Kayen et al. (2013), an average effective vertical stress of 100 kPa, and fines content of 6% has been assumed to keep the values within a reasonable range. Although the probabilistic liquefaction triggering curves for gravel developed in this study are similar to those for sands (Kayen et al., 2013) at lower V_{s1} values typical of looser gravels, the curves diverge as V_{s1} increases. For example, V_{s1} equals 275 m/s for the proposed $P_L = 50\%$ curve for gravel in this study at a CRR of 0.5 in comparison with a V_{s1} of only 225 m/s for the $P_L = 50\%$ curve for sand proposed by Kayen et al. (2013). This indicates that the probabilistic triggering curves for gravels from this study shift to the right relative to similar curves developed for sands as V_{s1} increases. This result indicates that gravels can still liquefy at V_{s1} values that would be high enough to preclude liquefaction in a sand. This does not mean that gravels are more or less likely to liquefy than sand, it simply means that for a comparable level of shaking, a higher V_{s1} is necessary to obtain the same probability of liquefaction for a sandy gravel than a sand. This result is consistent with liquefaction case histories in gravels reported by several investigators (Athanasopoulos-Zekkos et al., 2019, Stokoe et al., 1994; Chang, 2016; Rollins et al., 2020) as well as laboratory testing (Huber et al., 2017; 2018) where V_s-based triggering curves for sands would have incorrectly predicted no liquefaction.

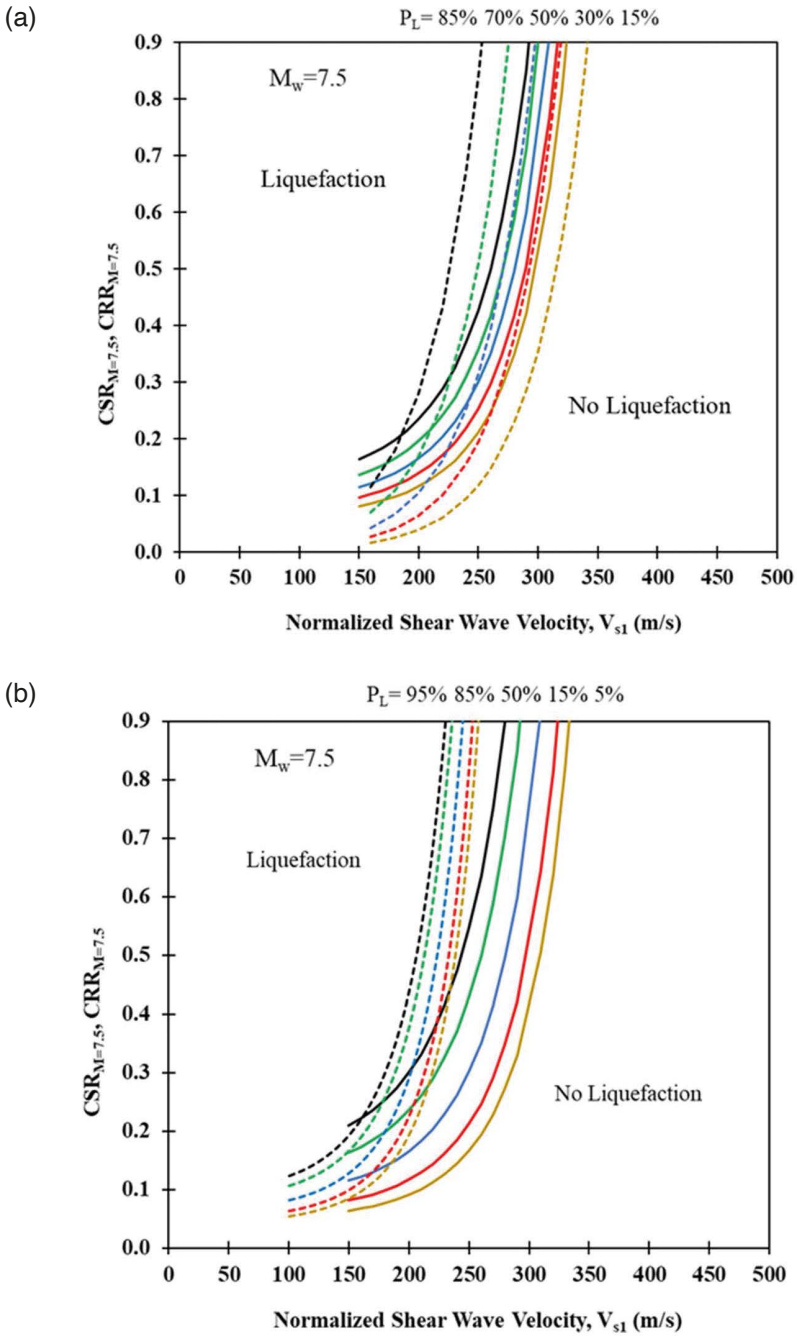

Figure 7. Liquefaction triggering curves from this study (solid lines) (a) relative to triggering curves proposed by Cao et al. (2011) (dashed lines) and (b) relative to triggering curves proposed by Kayen et al. (2013) for sands (dashed lines).

7. Development of Magnitude Scaling Factors

Most liquefaction triggering curves adjust the *CSR* for the earthquake magnitudes using a Magnitude Scaling Factor (MSF) to obtain an equivalent *CSR* for a M_W of 7.5 using the equation,

$$CSR_{M=7.5} = CSR/MSF \tag{13}$$

As a part of the present study, we have developed *MSF* models specifically for gravelly soils that may help improve liquefaction evaluation at some gravel sites, although more data from other earthquakes would be desirable. These

MSF curves are plotted and compared with several other *MSF* vs. M_w curves in Fig. 8.

To obtain the *MSF*, *CSR* values were first obtained from Eq. (10) for M_w 5.5 through 9 with an increment of 0.5 keeping N'_{120} and P_L constant. Then the *CSR*s for different magnitudes were divided by the *CSR* at $M_w = 7.5$ to obtain the magnitude scaling factor. The same process was then repeated by substituting different values of N'_{120} and P_L in Eq. (10) to obtain the variation of *MSF* with these variables. But notably, the *MSF* pattern did not show any variation with the DPT blow count (N'_{120}) and the probability of liquefaction (P_L). Based on this analysis the *MSF* for triggering analyses using the DPT blow counts can be computed as a function of magnitude with the best-fit exponential equation:

$$MSF = 7.258exp(-0.264M_w) \tag{14}$$

A similar approach was used to obtain the following best-fit exponential equation MSF equation for the V_S-based liquefaction triggering curve.

$$MSF = 10.667xp(-0.316M_w) \tag{15}$$

It can be observed that the *MSF* curves developed for gravelly soil fall about mid-way between the *MSF* vs. M_W curves for sand suggested by Idriss as endorsed by the NCEER/NSF liquefaction workshop (Youd et al., 2001) at the high end and the Kayen et al. (2013) curve at the low end. Hence, the proposed models for gravel appear to be reasonably consistent with existing *MSF* curves for sands.

Based on these *MSF* equations, the *CSRs* for all the case history data points have been converted to CSRs at $M_w = 7.5$ ($CSR_{Mw=7.5}$) and plotted with the newly developed triggering curves as shown in Figs. 5 and 6. Generally, the data points fall on the correct sides of the $P_L = 50\%$ curves for the liquefaction and no liquefaction points.

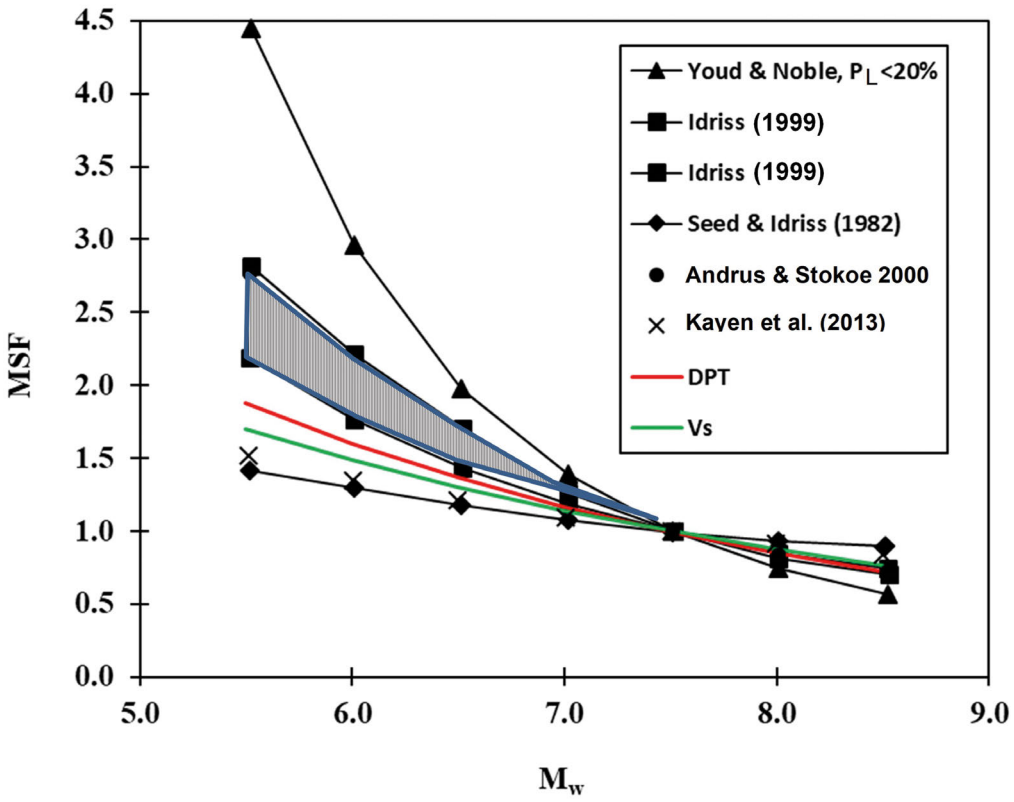

Figure 8. Comparison of *MSF* curves from logistical regression analysis of gravel liquefaction case histories based on the V_{s1} and DPT triggering curve with *MSF* curves proposed previously for gravel (Rollins et al. 2021; 2022).

8. Correlation Between Soil Properties and DPT N_{120} in Gravelly Soil

8.1 Correlation Between *Vs* and DPT N_{120}

In this study, many gravelly soil profiles were characterized by both DPT blow count (N'_{120}) and shear-wave velocity (V_S). Therefore, the potential for correlating V_S with DPT blow count was investigated. In total, 242 data points were collected from 54 different gravel sites around the world with V_S and DPT data. Although 64% of the data points come from the Chengdu plain of China, this database is comprised of a variety of environments including natural Holocene deposits from alluvial fans, glacial outwash, fluvial and glacio-fluvial deposits as well as man-made fills at ports and dams. In this dataset, the maximum depth is typically about 15 m and the maximum vertical effective stress, σ_{vo}', is about 250 kPa. The N_{120} values range from 2 to 55 while *Vs* values typically range from about 100 to 400 m/sec (Roy et al., 2023).

Although V_S has often been correlated with SPT blow count in sands, Rollins et al. (1998) developed correlations for gravels using equivalent SPT blow counts from Becker Penetration tests at dam sites. Rollins et al. (1998) found better correlations using the SPT N_{60} (blow count corrected to hammer delivering 60% of theoretical energy) and V_s values, uncorrected for vertical effective, while including the vertical effective stress as a separate variable.

In the current study, both the uncorrected N_{120} and the effective vertical stress (σ'_{vo}) have been considered as independent variables for predicting the uncorrected V_s. Based on a linear regression, the following equation for V_s. has been obtained

$$V_s = 108.25 + 3.66N_{120} + 0.642\sigma'_{vo} \tag{16}$$

A plot of the measured versus computed V_s using Eq. (16) is provided in Fig. 9 with data points separated by location. The data points typically plot within a range of ±25% of the perfect agreement line and appear to be symmetric about the line. In addition, none of the data points for the various locations appear to indicate aberrant behavior.

As part of this regression study, *p*-values for all the regression variables were calculated. A *p*-value measures the probability of obtaining the observed results, assuming that the null hypothesis is true. A *p*-value of 0.05 or lower is generally considered statistically significant and in this case the *p*-values are less than 0.0001 for all regression variables indicating that they are statistically significant. The regression coefficient (R^2) for this correlation is 0.72 with a root-mean-square error of 0.34. These regression metrics are typical of values for similar

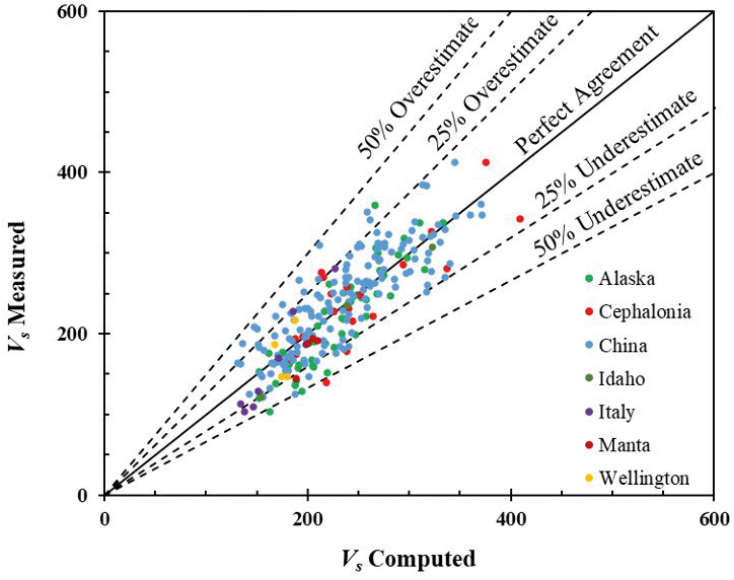

Figure 9. Comparison of measured V_S with V_S computed using Eq. (16) with DPT blow count (N_{120}) and vertical effective stress (σ'_v) as independent variables for the gravel database in this study (Roy et al., 2023).

correlations with sands. Regressions considering σ'_{vo} as a separate independent variable significantly improved the correlation coefficient compared to approaches where N'_{120} and V_{s1} were used in the regression. No improvement in the regression variables was found when using a log-linear correlation. In addition, separating the data points with respect to geological origin (e.g. alluvial, fluvial, man-made) did not significantly improve the correlations. However, it should be recognized that these gravel profiles were young Holocene age materials and older geological deposits might have different correlations as was observed by Rollins et al. (1998).

8.2 Correlations Between Relative Density and Drained Friction Angle

Based on Chinese experience with the DPT, Rollins et al. (2020) suggested that the relative density (D_r) in percent for gravelly soil could be estimated from the DPT blow count (N'_{120}) using the equation,

$$D_r = 100(N'_{120}/70)^{0.5} \tag{17}$$

Using the relative density obtained from Eq. (17), the drained friction angle (ϕ') of well-graded gravel (GW) can be obtained using the equation,

$$\phi' = 27.28 + 0.174D_r \tag{18}$$

where D_r is in percent. Likewise, the drained friction angle of poorly graded gravel (GP) can be obtained using the equation

$$\phi' = 26.98 + 0.15D_r \tag{19}$$

Lastly, the drained friction angle of well graded gravelly sand (SW) can be approximated using the equation,

$$\phi' = 26.78 + 0.134D_r \tag{20}$$

Equations 18, 19, and 20 were originally proposed by the US Navy (NAVFAC, 1982) in graphical form using soil types (e.g. GW, GP, SW) from the Unified Soil Classification System (ASTM, 2017). The US Navy does not have correlations for friction angle based on relative density for soils classifying as GM, GC, SM, and SC because (1) relative density is poorly defined for these materials and (2) the plasticity and fines content could produce large variations in the friction angle.

9. Conclusions

In this study, probabilistic liquefaction-triggering curves for gravelly soils based on the Dynamic Cone Penetration (DPT) test blow count (N'_{120}) and shear-wave velocity (V_s) were developed that can be used for liquefaction evaluation of gravelly soils for a wide range of earthquake magnitudes, tectonic settings, and geological environments. These curves are a significant step forward compared to those developed by Cao et al. (2011; 2013), as the total number of data points increased significantly. The N'_{120} and V_{s1} data were compiled from sites around the world where liquefaction did or did not occur during earthquake events. The expanded data set consisted of 174 V_s data points and 137 DPT data points from 17 different earthquakes in 10 different countries in a variety of geological environments.

Based on the results of the field studies and data analysis performed in this study, the following conclusions were drawn:

1) The increased number of liquefaction and no-liquefaction data points in the expanded data set better constrain the probabilistic liquefaction-triggering curves. Relative to the Cao et al. (2011) curves for V_s and

the Cao et al. (2013) curves for DPT, this shifted the $P_L = 85\%$ curve to the right and $P_L = 15\%$ curve to the left. The reduction in the range between the $P_L = 85\%$ and 15% curves indicates a considerable decrease in uncertainty, because false negative data points have less impact on the expanded data set. Shifting the $P_L = 15\%$ curve to the left is significant because this probability curve has been recommended for deterministic analyses (e.g. Kayen et al., 2013).

2) At lower V_{s1} values (≈150 m/s) and DPT blow counts less than 7, typical of looser gravels, the proposed triggering curves for gravel in this study start at a higher range of CSRs compared to the curves developed by Cao et al. (2011; 2013). This modification was necessary to produce agreement with the no-liquefaction points from the field case histories and brought the CSR values in line with the V_{s1} values for sand as predicted by the Kayen et al. (2013) probability curves.
3) Simplified *MSF* versus moment magnitude M_w equations were developed exclusively for gravel liquefaction. The *MSF* versus M_w curves plot about midway between similar curves proposed for sand. These results suggest that the effect of magnitude on liquefaction resistance is similar, but slightly different, for both sands and sandy gravels.
4) Although the probabilistic triggering curves for gravel are similar to those for sands (Kayen et al., 2013) at low V_{s1} values typical of loose gravels (≈150 m/s), they shift to the right as V_{s1} values increase. This indicates that gravels can still liquefy at V_{s1} values that would preclude liquefaction for sands. Therefore, using V_S-based triggering curves for sand when encountering gravels could incorrectly estimate gravel susceptible to liquefaction as being non-liquefiable.
5) A reasonable correlation has been developed for shear wave velocity (V_s) based on DPT blow count and vertical effective stress from 242 measurements. The correlation coefficient (R^2) was 0.72 and the error between measured and predicted V_s values was typically less than 25%.
6) Using the relative density obtained from the DPT, which is less affected by gravel particles, estimates of relative density can be obtained for cohesionless sand and gravel which can then be used to make an estimate of the drained friction angle.

Data availability statement. Data from critical layers in DPT database described in this paper can be downloaded from: https://doi.org/10.1061/(ASCE)GT.1943-5606.00026; while similar data from the Vs database can be accessed at: https://doi.org/10.1061/(ASCE)GT.1943-5606.0002784.

Acknowledgements. Funding for this study was provided by grant G16AP00108 from the US Geological Survey Earthquake Hazard Reduction Program and grants CMMI-1663546 and CMMI-663288 from the National Science Foundation. This funding is gratefully acknowledged. However, the opinions, conclusions and recommendations in this paper do not necessarily represent those of the sponsors. We express appreciation to Dr. Maurizio Vassallo, Dr. Giuseppe Di Giulio and Technologist Giuliano Milana of Istituto Nazionale di Geofisica e Vulcanologia for performing MASW testing to define V_S profiles at many gravel liquefaction sites for this study.

References

Andrus, R. D. (1994). In situ characterization of gravelly soils that liquefied in the 1983 Borah Peak earthquake, Ph.D. Dissertation, Civil Engineering Dept., Univ. of Texas at Austin, 579 pp.

Andrus, R. D. and K. H. Stokoe II (2000). Liquefaction resistance of soils from shear-wave velocity, J. Geotech. Eng., 126 (11), doi:10.1061/(ASCE)1090-0241(2000)126:11(1015).

ASTM (2018). Standard test method for use of the dynamic cone penetrometer in shallow pavement applications. ASTM D6951/D6951M-18. West Conshohocken, PA.

ASTM (2017). D2487-17 Standard practice for classification of soils for engineering purposes (Unified Soil Classification System, West Conshohocken, PA.

Athanasopoulos-Zekkos, A., D. Zekkos, K. M. Rollins, J. Hubler et al. (2019). Earthquake performance and characterization of gravel-size earth fills in the ports of Cephalonia, Greece, following the 2014 Earthquakes. Earthquake Geotechnical Engineering for Protection and Development of Environment and Constructions, Procs. 7th Intl. Conf. on Earthquake Geotechnical Engineering, Taylor and Francis, 212-1219.

British Standard (2012). Geotechnical investigation and testing – Field testing – Part 2: Dynamic probing BS ENISO 22476-2:2005+A1:2011.

Boulanger, R. W. and I. M. Idriss (2014). CPT and SPT based liquefaction triggering procedures. Center of Geotechnical Modeling, Univ. of California-Davis, Report No. UCD/CGM-14/01.

Cao, Z., T. L. Youd and X. Yuan (2011). Gravelly soils that liquefied during 2008 Wenchuan, China Earthquake, Ms = 8.0, Soil Dyn. Earthq. Eng., 31(8), 1132-1143, doi:10.1016/j.soildyn.2011.04.001.

Cao, Z., X. Yuan, T. L. Youd and K. M. Rollins, (2012). Chinese Dynamic Penetration tests (DPT) at liquefaction sites following 2008 Wenchuan Earthquake, Proc., 4th Int. Conf. on Geotechnical and Geophysical Site Characterization, Taylor & Francis Group, London, 1499-1504.

Cao, Z., T. Youd and X. Yuan, (2013). Chinese Dynamic Penetration Test for liquefaction evaluation in gravelly soils. J. Geotech. Eng., 139(8), 1320-1333,10.1061/(ASCE)GT.1943-5606.0000857.

Chang, W.J. (2016). Evaluation of liquefaction resistance for gravelly sands using gravel content-corrected shear-wave velocity, J. Geotech. Eng., 142(5), doi:10.1061/(ASCE)GT.1943-5606.0001427.

Chen, L., X. Yuan, Z. Cao, R. Sun et al. (2018). Characteristics and triggering conditions for naturally deposited gravelly soils that liquefied following the 2008 Wenchuan M_w 7.9 Earthquake Spectra, 34(3), 1091-1111, doi:10.1193/032017EQS05.

Chinese Design Code (2001). Design code for building foundation of Chengdu region [In Chinese] DB51/T5026-2001. Sichuan Province, Chengdu, China: Administration of Quality and Technology.

Cubrinovski, M., A. Rhodes, N. Ntritsos and S. Van Ballegooy (2017). System response of liquefiable deposits, Soil Dyn. Earthq. Eng., 124, 212-229, doi:10.1016/j.soildyn.2018.05.013.

DeJong, J. T., M. Ghafghazi, A. P. Sturm, D. W. Wilson et al. (2017). Instrumented Becker Penetration Test. I: Equipment, Operation, and Performance. J. Geotech. Eng., 143(9), doi:10.1061/(ASCE)GT.1943-5606.0001717.

Golesorkhi, R. (1989). Factors influencing the computational determination of earthquake-induced shear stresses in sandy soils. PhD dissertation, University of California, Berkeley, California.

Harder, L. F., Jr. and H. B. Seed (1986). Determination of penetration resistance for coarse-grained soils using the Becker Hammer Drill. College of Engineering, University of California, Berkeley, Calif. Rep. No. UCB/EERC-86/06. May.

Harder, L. F. (1997). Application of the Becker Penetration Test for evaluating the liquefaction potential of gravelly soils. NCEER Workshop on Evaluation of Liquefaction Resistance, held in Salt Lake City, Utah.

Hubler, J., A. Athanasopoulos-Zekkos and D. Zekkos (2018). Monotonic and cyclic simple shear response of gravel-sand Mixtures, Soil Dyn. Earthq. Eng., 115, 291-304, doi:10.1016/j.soildyn.2018.07.016.

Hubler, J., A. Athanasopoulos-Zekkos and D. Zekkos (2017). Monotonic, cyclic and post-cyclic simple shear response of three uniform gravels in constant volume conditions, J. Geotech. and Geoenviron Eng. ASCE, Washington, DC, 143(9).

Idriss, I. M. (1999). An update to the Seed-Idriss simplified procedure for evaluating liquefaction potential. Procs. TRB Workshop on New Approaches to Liquefaction, Publication No. FHWA-RD-99-165, Federal Highway Administration.

Idriss, I. and R. W. Boulanger (2008). Soil liquefaction during earthquakes. Earthquake Engineering Research Institute. Oakland, California, Monograph.

Iqbal, M. S. (2004) Discrete Element Modeling of Cone Penetration Testing in Coarse Grain Soils, MS Thesis, Univ. of Alberta, Edmonton, Canada, 136 p.

Kayen, R., R. E. S. Moss, E. M. Thompson and R. B. Seed et al. (2013). Shear-wave velocity-based probabilistic and deterministic assessment of seismic soil liquefaction potential, J. Geotech. and Geoenviron, 139(3), 407-419, doi:10.1061/(ASCE)GT.1943-5606.00007.

Morales, C., C. Ledezma, E. Saez and S. Boldrini et al. (2020). Seismic failure of an old pier during the 2014 M_w 8.2, Pisagua, Chile earthquake, Earthquake Spectra, 36(2), 880-903, doi:10.1177/8755293019891726.

NAVFAC (1982). Soil Mechanics, DM-7.2, US Navy Facilities.

Ohta, Y. and N. Goto, (1978). Physical background of the statistically obtained S-wave velocity equation in terms of soil indexes, ButsuriTanko(Geophysical Exploration), Tokyo, Japan, 31(1), 8-17 (In Japanese).

Rollins, K. M., M. Evans, N. Diehl and W. Daily (1998). Shear modulus and damping relationships for gravels, J. Geotech. and Geoeviron. Eng., ASCE, 124(5), 396-405, doi:10.1061/(ASCE)1090-0241(1998)124:5(396).

Rollins, K. M., C. Ledezma, G. Montalva, A. Becerra et al. (2014). Geotechnical Aspects of April 1, 2014, M8.2 Iquique, Chile Earthquake. GEER Association Report No. GEER-038, 77 p. Version 1.2: October 22, 2014.

Rollins, K. M., S. Amoroso, G. Milan, L. Minerelli et al. (2020). Gravel liquefaction assessment using the dynamic cone penetration test based on field performance from the 1976 Friuli earthquake, J. Geotech. Geoenv. Eng., 146(6), doi:10.1061/(ASCE)GT.1943-5606.00022.

Rollins, K. M., J. Roy, A. Athanasopoulos-Zekkos, D. Zekkos et al. (2021). New dynamic cone penetration test-based procedure for liquefaction triggering assessment of gravelly soils, J. Geotech. Geoenv. Eng. ASCE, 147(12), doi:10.1061/(ASCE)GT.1943-5606.000268.

Rollins, K. M., J. Roy, A. Athanasopoulos-Zekkos, D. Zekkos et al. (2022). A New V_s-based liquefaction triggering procedure for gravelly soils, J. Geotech. Geoenv. Eng., 148(6), doi:10.1061/(ASCE)GT.1943-5606.0002784.

Rollins, K., S. Amoroso, A. Walburger, G. di Giulio et al. (2024). Liquefaction assessment at gravel sites in Croatia based on V_s and DPT blow count." Procs. 7th Intl. Conf. on Geophysical and Geotechnical Site Characterization, 8 p.

Roy, J. and K. M. Rollins (2022). Effect of hydraulic conductivity and impeded drainage on the liquefaction potential of gravelly soils. Canadian Geotechnical J., Canadian Science Publishing, 58(11), 1950-1968, doi:10.1139/cgj-2021-0579.

Roy, J., K. Rollins, A. Athanasopoulos-Zekkos and D. Zekkos (2023). Correlation between shear wave velocity and dynamic cone resistance for gravelly soil, J. Geotech. Geoenviron. Eng., 149(9), 10 p., doi:10.1061/JGGEFK.GTENG-11254.

Roy, J., K. Rollins, R. Dakal and M. Cubrinovski (2023). A comparative study of the DPT and CPT in evaluating liquefaction potential for gravelly soil at the Port of Wellington, J. Geotech. Geoenv. Eng., 149(11), doi:10.1061/JGGEFK.GTENG-10769.

Sebastian Lopez, J., X. Vera-Grunauer, K. Rollins and G. Salvatierra (2018). Gravelly soil liquefaction after the 2016 Ecuador earthquake. Procs. Geotechnical Earthquake Engineering and Soil Dynamics V, 13 p., doi:10.1061/9780784481455.027.

Seed, H. B. and I. M. Idriss (1971). Simplified procedure for evaluating soil liquefaction potential, J. Geotech. Engrg. Div., 97(9),1249-1273, doi:10.1061/JSFEAQ.000166.

Seed, H. B. and I. M. Idriss. (1971). Simplified procedure for evaluating soil liquefaction potential, J. Soil Mech. Found. Div. 97 (9), 1249-1273, doi:10.1061/JSFEAQ.0001662.

Seed, H. B., K. Tokimatsu, L. F. Harder and R. M. Chung (1985). Influence of SPT procedures in soil liquefaction resistance evaluations, J. Geotech. Eng., 111(12), doi:10.1061/(ASCE)0733-9410(1985)111:12(1425).

Sirovich, L. (1996). Repetitive liquefaction at gravelly site and liquefaction in overconsolidated sands, Soils and Foundations, (36)4, 23-34, 10.3208/sandf.36.4_23.

Sykora, D. W. (1987). Creation of a database of seismic shear wave velocities for correlation analysis, Geotech. Lab. Misc. Paper GL-87-26, U.S. Army Engr. Waterways Experiment Station, Vicksburg, Miss.

Stokoe, K. H. II, S. G. Wright, J. A. Bay and J. M. Roesset (1994). Characterization of geotechnical sites by SASW method, ISSMFE, Technical Committee #10 for XIII ICSMFE, Geophysical Characterization of Sites, A. A. Balkema Publishers/Rotterdam & Brookfield, Netherlands,15-25.

Vantassel, J. P. and B. R. Cox (2022). SWprocess: a workflow for developing robust estimates of surface wave dispersion uncertainty, J. Seismol., 26, 731-756, doi:10.1007/s10950-021-10035-y.

Weston, T. R. (1996). Effects of grain size and particle distribution on the stiffness and damping of granular soils at small strains. MS thesis, Dept. of Civil & Env. Eng., University of Texas, Austin, Texas.

Worden, C. B., D. J. Wald, T. L. Allen, K. Lin et al. (2010). Integration of macroseismic and strong-motion earthquake data in ShakeMap for real-time and historic earthquake analysis. USGS website, http://earthquake.usgs.gov/earthquakes/shakemap/.

Yegian, M. K., V. G. Ghahraman and R. N. Harutiunyan (1994). Liquefaction and embankment failure case histories, 1988 Armenia earthquake, J. Geotech. Eng., 120(3), doi:10.1061/(ASCE)0733-9410(1994)120:3(581).

Youd, T. L. and S. K. Noble (1997). Liquefaction criteria based on statistical and probabilistic analyses. Proc., NCEER Workshop on Evaluation of Liquefaction Resistance of Soils, NCEER Technical Rep. No: NCEER-97 (Vol. 22, pp. 201-205).

Youd, T. L., I. M. Idriss, R. D. Andrus, I. Arango et al. (2001). Liquefaction resistance of soils: Summary Report from the 1996 NCEER and 1998 NCEER/NSF Workshops on evaluation of liquefaction resistance of soils. J. Geotech. Eng., 10.1061/(ASCE)1090-0241(2001)127:10(817).

***CORRESPONDING AUTHOR: Kyle ROLLINS**,
Brigham Young University, Civil & Construction Engineering Dept., Provo, Utah, USA
e-mail: rollinsk@byu.edu